The impact of global changes in near-term climate forcers on East Africa's climate

Ronald Opio[1*], Isaac Mugume[1,2], Joyce Nakatumba-Nabende[3], Alex Nimusiima[1] and Isaac Tom Okurut[4]

Abstract

Climate change and air pollution are two interconnected daunting environmental challenges of the twenty-first century. Globally, stringent public health and environmental policies are set to mitigate the emissions of near-term climate forcers (NTCFs) because they double as air pollutants. While the global climate impact of NTCF mitigation has been investigated using coarse resolution climate models, the fine scale regional climate impacts over East Africa are not fully known. This study presents the first 2021–2055 downscaled model results of two future scenarios which both have increasing greenhouse gas emissions but with weak (SSP3-7.0) versus strong (SSP3-7.0_lowNTCF) levels of air quality control. NTCF mitigation is defined here as SSP3-7.0_lowNTCF–SSP3-7.0. The results reveal that NTCF mitigation could cause an increase in annual mean surface temperature ranging from 0.005 to 0.01 °C decade^{-1} over parts of Kenya, Ethiopia and Somalia. It could also cause an increase in annual mean precipitation ranging from 0.1 to 1 mm month^{-1} decade^{-1} over parts of Uganda, Kenya, Tanzania, South Sudan and Ethiopia. Majority of the precipitation increase is projected to occur during the MAM season. On the other hand, Zambia, Malawi and southern Tanzania could also experience a decrease in annual mean precipitation by up to 0.5 mm month^{-1} decade^{-1}. Majority of this decrease is projected to occur during the DJF season. These findings suggest that pursuing NTCF mitigation alone while ignoring greenhouse gas emissions will cause additional climate change over East Africa. Mitigating both of them concurrently would be a better policy option.

Keywords Climate change, Near-term climate forcers, Air pollution, CMIP6, Downscaling, WRF

Introduction

Near-term (short-lived) climate forcers (NTCFs) are atmospheric chemistry species which exert a modifying effect on climate within two decades after they have been emitted or formed (Szopa et al. 2021). This is due to their short atmospheric residence times that range from hours to a few months for most NTCFs. Direct NTCFs

such as aerosols, ozone (O_3) and methane (CH_4) exert a radiative forcing which influences the radiation budget of the atmosphere, while indirect NTCFs such as nitrogen oxides (NO and NO_2), sulphur dioxide (SO_2), carbon monoxide (CO) and non-methane volatile organic compounds (NMVOCs) are precursors to the direct NTCFs. Through complex chemical processes, the indirect NTCFs control the atmospheric abundance of the direct NTCFs. For example, ozone is formed through a photochemical reaction between NO_x and volatile organic compounds (Li et al. 2022; Lu et al. 2019), while sulphate and nitrate aerosols are formed through the oxidation of SO_2 and NO_2, respectively (Jacob 2021).

Besides their influence on climate, NTCFs are also air pollutants, and they trigger and/or exacerbate respiratory illnesses like lung cancer, acute lower respiratory infection and chronic obstructive pulmonary disease (World

*Correspondence:
Ronald Opio
opioronald123@gmail.com
[1] Department of Geography, Geo-Informatics and Climatic Sciences, Makerere University, 7062, Kampala, Uganda
[2] Directorate of Forecasting Services, Uganda National Meteorological Authority, 7025, Kampala, Uganda
[3] Department of Computer Science, Makerere University, 7062, Kampala, Uganda
[4] Department of Environmental Management, Makerere University, 7062, Kampala, Uganda

Opio *et al. Environmental Systems Research*   (2023) 12:16

Page 2 of 16

Health Organization 2018). They are also associated with cardiovascular illnesses such as coronary artery disease, cardiac arrest, and heart failure (Miller and Newby 2020). This pollution commonly takes the form of tropospheric ozone and particulate matter with a diameter of less than 2.5 μm ($PM_{2.5}$). A small contribution also comes from the precursor gases such as NO_2, SO_2 and CO (Fowler et al. 2020; Pozzer et al. 2023). Globally, ambient air pollution is considered the leading environmental risk factor, causing more than 50% of the deaths which is approximately 4.2 million deaths yearly (Cohen et al. 2017; Pozzer et al. 2023). Due to this, environmental and public health policies now target the reduction of these air pollutants to improve air quality.

Currently, NTCF emissions are concentrated in highly populated regions of the world. These include China, India, eastern United States, and Europe (Hoesly et al. 2018). Africa is also an important emission source for black carbon (BC) and organic (OC) aerosols which are associated with biomass burning. Major emissions of NO_x and SO_2 are also concentrated over the global oceans, along the international shipping routes (Hoesly et al. 2018). Since the year 2000, Eastern and Southern Asia have had the highest levels of NTCF emissions due to industrial development (Szopa et al. 2021). By contrast, over North America and Europe, the emissions of some NTCFs such as NO_2 and SO_2 have declined in the past decade, 2010 to 2019 (Aas et al. 2019; Jiang et al. 2018; Miyazaki et al. 2017). China also had major SO_2 declines within that decade (Zheng et al. 2018). CO abundance is also on a decline globally (Buchholz et al. 2021). These declines were all due to adoption of policies that restrict the emission of NTCFs.

Adoption of these policies will cause future reductions in the emissions and abundances of NTCFs, which will have a small but important impact on climate (Allen et al. 2020). This scientific domain is being explored using model simulations from coupled chemistry-climate models such as version 2 of the Community Earth System Model (Emmons et al. 2020; Gettelman et al. 2019; Tilmes et al. 2019) and the Max Planck Institute Earth System Model (Tegen et al. 2019). First, idealized experiments have been used to investigate the climate impact that will arise from the total removal of anthropogenic emissions of selected NTCFs (Baker et al. 2015; Kasoar et al. 2016; Lelieveld et al. 2019; Samset et al. 2018). Secondly, coordinated modeling experiments have been carried out under the Aerosol Chemistry Model Intercomparison Project (AerChemMIP) as part of phase 6 of the Coupled Model Intercomparison Project (CMIP6). AerChemMIP is designed to quantify the climate and air quality impacts of aerosols and chemically reactive gases, specifically, NTCFs (Collins et al. 2017). The latter

is more realistic as it offers a variety of model simulations which are important for quantifying model uncertainty.

To provide context of the full impact that reductions in NTCFs will have on climate, AerChemMIP experiments are compared against experiments from the Scenario Model Intercomparison Project (ScenarioMIP) (O'Neill et al. 2016). Specifically, two future scenarios are compared, these are; SSP3-7.0 from ScenarioMIP and SSP3-7.0_lowNTCF from AerChemMIP. SSP3-7.0 has weak air quality control and high NTCF emissions while SSP3-7.0_lowNTCF has strong air quality control and low NTCF emissions. The mathematical difference between these two experiments is then used to reveal the climate impact (Allen et al. 2020; Collins et al. 2017; Hassan et al. 2022). It is important to note that these experiments have the same levels of well-mixed greenhouse gases and CH_4. Therefore, the climate impact revealed here is due to changes in only non-methane NTCFs.

The first multi-model global assessment of this climate impact was done by Allen et al. (2020) and it revealed that the mitigation of non-methane NTCF emissions would cause a future increase in surface temperature and precipitation due to the net warming effect that the reduction in aerosols would induce. This would also be accompanied by an increase in the number of hottest and wettest days. Over Africa, Allen et al. (2020) noted that the bulk of the precipitation increase would occur in East Africa (Fig. 1). Though useful, their results were based on coarse resolution models which could only offer limited insight. Exploring this problem using model simulations at finer spatial scales might be reveal new insights. Therefore, this study sought to further investigate these projected changes in temperature and precipitation over East Africa by dynamically downscaling one of the CMIP6 global climate model (GCM) experiments analyzed by Allen et al. (2020). This is the first study to downscale these model experiments over East Africa.

Since most GCM output is at coarse spatial scales of between 100 and 500 km, they are unable to accurately resolve local features such complex topography, mesoscale circulations, land use/land cover and coastlines, all of which are important in determining local climate patterns (Giorgi and Gutowski 2015; Walton et al. 2015; Xu et al. 2019). Due to this, GCM output only offers limited insight into local climate dynamics. To improve their utility, downscaling is carried out to provide finer detail in the spatial and temporal patterns, which offers several advantages. For example, the finer resolution and improved representation of topography allows for better representation of near-surface temperature gradients and the rain shadow effect that is associated with steep mountain ranges (Di Luca et al. 2012, 2015). Typically, for the GCM output to be useful for local applications,
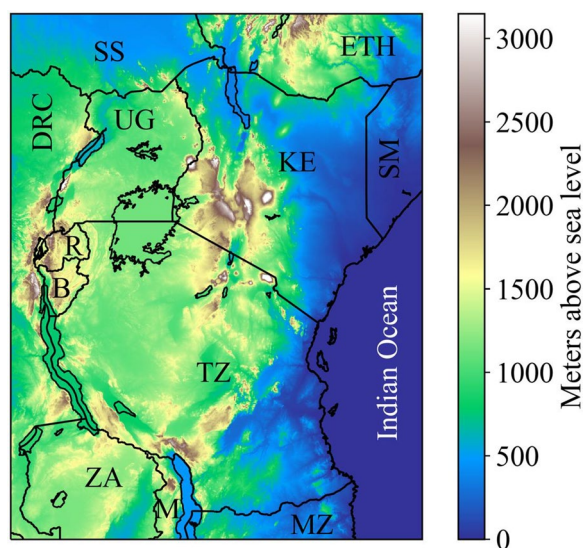
Fig. 1 Map of East Africa showing its complex topography and countries. These are; Uganda (UG), Kenya (KE), Tanzania (TZ), Rwanda (R), and Burundi (B) along with the neighboring regions including South Sudan (SS), Democratic Republic of Congo (DRC), Zambia (ZA), Malawi (M), Mozambique (MZ), Somalia (SM) and Ethiopia (ETH). This is also the simulation domain used for the downscaling process in WRF

it has to be downscaled to a resolution of at least 25 km or something finer than that. This is the based on recent downscaling studies (Fernández-Alvarez et al. 2023; Rahimi et al. 2020; Xu 2021; Yang et al. 2023; Ye et al. 2022; Yu et al. 2023). Over East Africa, the impact that global mitigation of NTCFs will have on temperature and precipitation at such fine spatial scales is not fully known. This study is the first attempt to investigate this impact.

Data and methods
Study area
East Africa's climate requires keen scientific study because of the complex mix of factors that influence the region's climate. For example, the biannual crossing of the Intertropical Convergence Zone (ITCZ) creates a bimodal precipitation cycle, consisting of the long precipitation season that occurs from March to May (MAM) and the short precipitation season that occurs from September to November (SON) (Nicholson 2019). The El Niño Southern Oscillation (ENSO) and the Indian Ocean Dipole (IOD) enhance precipitation receipts over East Africa during SON, thus creating more interannual precipitation variability during SON compared to MAM (Nicholson 2019; Wenhaji Ndomeni et al. 2018). The other important factors include the Madden–Julian Oscillation, tropical cyclones, and the existence of mountains and large inland lakes (Finney et al. 2020; Nicholson

2017; Walker et al. 2020). There is also the East African climate paradox that has further confounded the study of the region's climate (Mölg and Pickler 2022; Wainwright et al. 2019).

The historical climate trends show that East Africa's precipitation has remained the same in the majority of the region and only changed in a few areas. For example, during the period 1981 to 2017, a precipitation increase of between 3 and 15 mm year^{-1} occurred in the region between Uganda and Kenya that surrounds Lake Victoria. A precipitation decrease of 20 mm year^{-1} occurred near Mt. Kilimanjaro in northern Tanzania and other declines in precipitation of ~4 to 10 mm year^{-1} occurred over small regions in central Kenya, central Uganda, southwest Tanzania, and western Rwanda (Gebrechorkos et al. 2019a; Muthoni et al. 2019). Over Uganda alone, a small increasing trend in precipitation was identified starting in 2010 (Ngoma et al. 2021). On the other hand, East Africa's temperature has shown an increasing trend in the majority of the region. For the 1979 to 2010 period, this increase reached 1.9 °C (Gebrechorkos et al. 2019a, b).

Concerning the future climate projections, the majority of the CMIP6-based climate modeling studies over the region have focused on the role of well-mixed greenhouse gases (Akinsanola et al. 2021; Ayugi et al. 2021, 2022a; b; Makula and Zhou 2022; Vashisht et al. 2021). By contrast, this study has investigated the role of NTCFs since they also pose a threat to East Africa's climate.

Data
Much as statistical (Thrasher et al. 2022) and machine learning-based (Baño-Medina et al. 2020) downscaling is possible, this study preferred a physics-based dynamical downscaling because its results are physically consistent and scientifically reliable. Therefore, this study downscaled the Max Planck Institute Earth System Model (MPI-ESM1-2-HAM) using a physics-based regional climate model, that is, the Weather Research and Forecasting (WRF) model. The downscaling was from 250 to 23 km (Fig. 2). The two models and their data are described below.

MPI-ESM1-2-HAM model
The MPI-ESM1-2-HAM model is a fully coupled ocean-atmosphere model which was run for CMIP6 by the HAMMOZ Consortium (Mauritsen et al. 2019; Neubauer et al. 2019). The model's atmosphere component was set up with a horizontal resolution of 250 km and 47 vertical levels up to 0.01 hPa (Neubauer et al. 2019). This model used identical ozone levels in both SSP3-7.0 and SSP3-7.0_lowNTCF experiments and only aerosol levels were allowed to change. Therefore, the differences
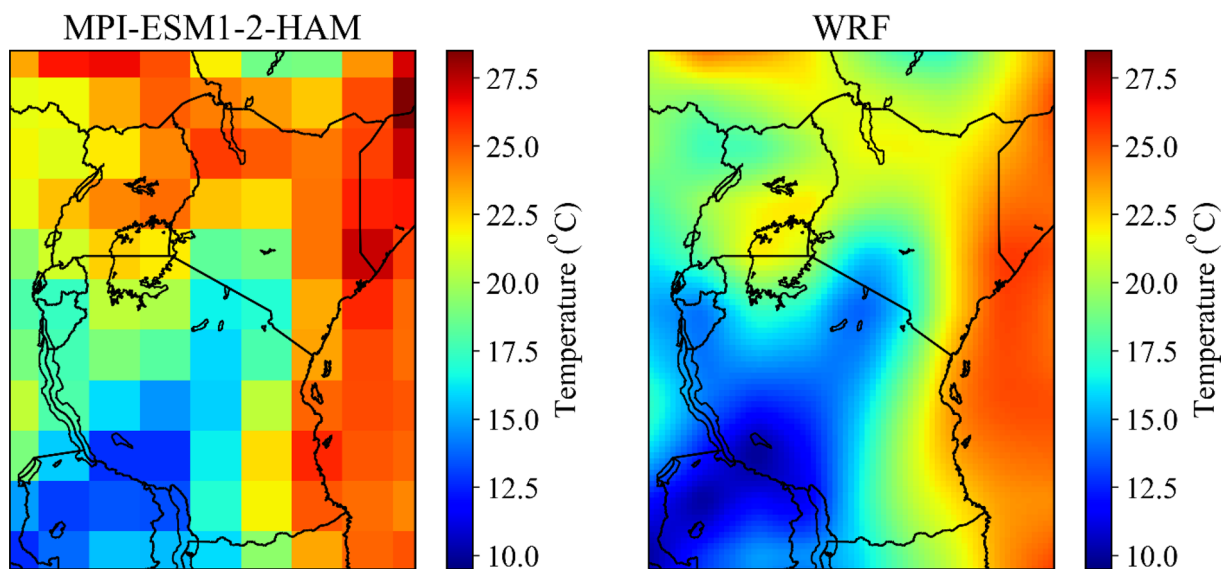
Fig. 2 Near surface air temperature on 1st July 2030 as simulated by MPI-ESM1-2-HAM (250 km) and WRF (23 km) for SSP3-7.0_lowNTCF

Table 1 The nine models that performed both SSP3-7.0 and SSP3-7.0_lowNTCF experiments under CMIP6

Model	References
BCC-ESM1	Wu et al. (2019, 2020)
CESM2-WACCM	Emmons et al. (2020), Tilmes et al. (2019), Gettelman et al. (2019)
CNRM-ESM2-1	Séférian et al. (2019), Michou et al. (2020)
GFDL-ESM4	Horowitz et al. (2020), Dunne et al. (2020)
MIROC6	Takemura et al. (2005, 2009), Tatebe et al. (2019)
MPI-ESM1-2-HAM	Mauritsen et al. (2019), Neubauer et al. (2019), Tegen et al. (2019)
MRI-ESM2-0	Yukimoto et al. (2019)
Nor-ESM2-LM	Seland et al. (2020)
UKESM1-0-LL	Sellar et al. (2019)

in climate generated here were only due to changes in aerosol amounts. Further, the experiments were only run from 2015 to 2055 because this is the time period during which changes in aerosol and precursor emissions are expected to be significant (Collins et al. 2017).

Among the nine coupled chemistry-climate models (Table 1) that performed both SSP3-7.0 and SSP3-7.0_ lowNTCF experiments, only MPI-ESM1-2-HAM was selected for the downscaling in this study. This model was the only one that provided outputs for both experiments at a 6-hourly temporal resolution. Data at such a high temporal resolution was necessary for generating realistic boundary conditions for driving WRF. The variables used were the eastward and northward near surface wind, eastward and northward wind, near surface specific humidity, specific humidity, soil temperature, moisture in the upper portion of the soil column, surface air pressure, sea level pressure, surface temperature, near

surface air temperature, air temperature and geopotential height. All these data were downloaded from the Earth System Grid Federation (ESFG) database hosted at the Lawrence Livermore National Laboratory.[1] To be suitable input data for WRF, the MPI-ESM1-2-HAM variables were preprocessed into 6-hourly intermediate files, with each file containing all the variables. This was done in Python 3.9.7. Thereafter, the data were interpolated onto the WRF model grid using the *metgrid* function within the WRF preprocessing system.

In addition to the meteorological variables, the model output for $PM_{2.5}$ mass mixing ratio in lowest model layer was also obtained and analyzed to show the difference in $PM_{2.5}$ aerosol burden between SSP3-7.0 and SSP3-7.0_ lowNTCF. The data were converted from mass mixing

---

[1] https://esgf-node.llnl.gov/search/cmip6/.

ratio (kg kg^{-1}) to concentration (µg m^{-3}) following the procedure described by Gomez et al. (2023). The quantity was multiplied by air density which was calculated as in Eq. (1). The unit of pressure was Pascals, while that of temperature was Kelvins. The dry gas constant was 287 JK^{-1} kg^{-1}.

$$Air\,density = \left(\frac{Surface\,pressure}{Surface\,temperature \times Dry\,gas\,constant} \right) \times 1e^9 \tag{1}$$

Weather Research and Forecasting (WRF) model
Version 4.3 of the WRF model, Advanced Research WRF dynamics solver (Skamarock et al. 2019) was used for the downscaling experiments. It is a regional atmospheric modeling system based on the physical equations. WRF is designed with Arakawa C-grid staggering, 2nd and 3rd order Runge–Kutta time integration, and a terrain-following hybrid sigma-pressure vertical coordinate system (Skamarock et al. 2019). For this study, the model was set up with one domain (Fig. 1) at a horizontal resolution of 23 km (110 × 100 grids) and a vertical resolution of 31 eta levels ending at 50 hPa at the top.

The model was set up with the Lin microphysics (Lin et al. 1983), Grell 3-D cumulus parameterization (Grell and Dévényi 2002), the Noah land surface model (Chen and Dudhia 2001), Yonsei University Scheme for the boundary layer parameterization (Hong et al. 2006) and the Rapid Radiative Transfer Model for GCMs (Iacono et al. 2008) for both shortwave and longwave radiation parameterization. These parameterization choices were based on previous studies focused on East Africa (Nooni et al. 2022; Otieno et al. 2019). The model was run from 2021 to 2055 at intervals of 1 month while using 1 extra day for model spin-up.

WRF generates about 255 different output variables, but the ones that are associated with precipitation are the accumulated total cumulus precipitation and the accumulated total grid scale precipitation. The two components were summed up to obtain the total accumulated precipitation value that was analyzed here. Furthermore, the variable directly associated with surface temperature is the 2-m temperature variable. The other variables include the eastward and northward surface wind, eastward and northward wind at model levels, surface pressure, total pressure, surface mixing ratio and geopotential height. The full list of variables can be found in Skamarock et al. (2019).

SSP3-7.0 and SSP3-7.0_lowNTCF emissions
The SSP3-7.0 scenario assumes a future with high inequality between and within countries, the so-called 'regional rivalry'. It is envisaged that there will be weak and non-uniform air pollution legislation and no greenhouse gas mitigation (Fujimori et al. 2017). Consequently, the world under this scenario will have the highest emission levels of NTCFs and substantially high levels of greenhouse gases. The latter is the reason why some literature refer to this scenario as 'lacking climate policy' (Fujimori et al. 2017; Gidden et al. 2019). By contrast, the SSP3-7.0_lowNTCF scenario uses the same assumptions as SSP3-7.0 except that it assumes a world where stringent policies are enacted to mitigate NTCFs but while completely ignoring greenhouse gas emissions. Therefore, NTCF emissions decrease while greenhouse gas emissions continue to increase (Gidden et al. 2019). SSP3-7.0_lowNTCF assumptions for NTCFs are similar to those under the sustainability scenario, SSP1. For example, it uses the same CH_4 emission reduction rates and the same emissions factors for the other air pollutants, that is, NO_x, CO, BC, OC, NH_3, VOC and sulfur (Gidden et al. 2019). For this study, the NTCF emissions used for SSP3-7.0 and SSP3-7.0_lowNTCF were obtained from the input forcing data for CMIP6 (Gidden et al. 2018a, b). These data were also downloaded from the ESFG database hosted at the Lawrence Livermore National Laboratory.[2] The data for 2015 to 2055 were plotted to show the difference in NTCF emissions between the two experiments.

Methods
Difference variable
The difference variable (Willmott et al. 1985) was applied to the model output from both SSP3-7.0 and SSP3-7.0_lowNTCF as demonstrated in earlier studies (Allen et al. 2020; Collins et al. 2017; Hassan et al. 2022). The effect of NTCF mitigation was calculated as shown in Eq. 2.

$$NTCF\,mitigation = SSP3\_7.0\_lowNTCF - SSP3\_7.0 \tag{2}$$

Mann–Kendall trend test and Sen's slope estimator
Two non-parametric tests, that is, Mann–Kendall (Kendall 1975; Mann 1945) and Sen's slope estimator (Sen 1968) were applied in both spatial and temporal context to test for the existence of a trend at a significance level of 95%. This implies that the standard normal statistic, Z would have limits as +1.96 and −1.96. These methods have previously been applied in a similar way to meteorological time series data and were found adequate in revealing the trend (Alemu et al. 2015; Gebrechorkos et al. 2019a; Gocic and Trajkovic 2013; Muthoni et al. 2019; Ngoma et al. 2021; Onyutha 2016). In this study,
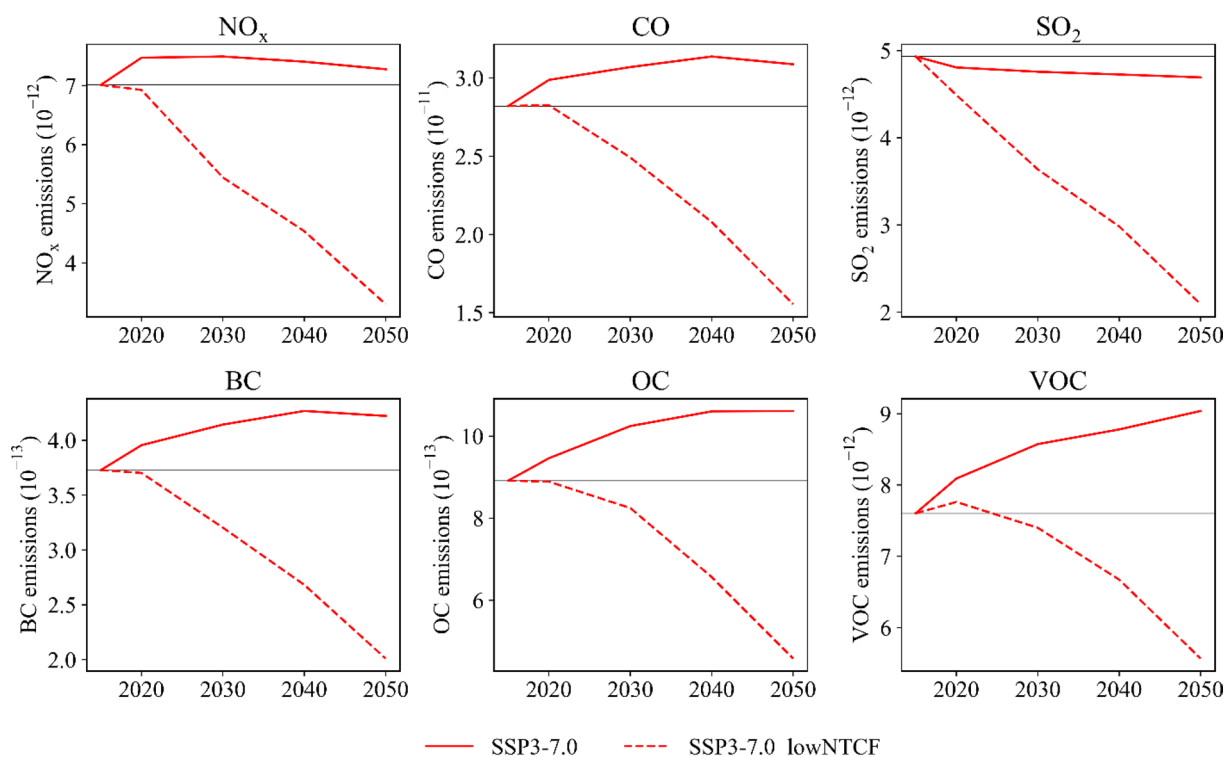
---

[2] https://esgf-node.llnl.gov/projects/input4mips/.

Fig. 3 Global average anthropogenic emission estimates (kg m^{-2} s^{-1}) of major NTCFs from 2015 to 2050. These were the emission trajectories used for SSP3-7.0 and SSP3-7.0_lowNTCF experiments. The horizontal black line shows the 2015 value

the methods were applied to PM$_{2.5}$, temperature and precipitation data. All the data covered 35 years (2021 to 2055). For temperature and precipitation, the temporal trends were only done for countries whose geographical extent was fully contained within the study area. These were; Uganda, Kenya, Tanzania, Rwanda and Burundi. For the neighboring countries; DRC, South Sudan, Ethiopia, Somalia, Mozambique, Malawi and Zambia, the temporal trend statistic would not make complete scientific sense as only small portions of the geographical areas of these countries were contained within the study region.

Results and discussion

SSP3-7.0 and SSP3-7.0_lowNTCF emission differences

Figure 3 shows the global average emission estimates of major NTCFs from 2015 to 2050. Under SSP3-7.0, the emissions of CO and BC are projected to increase until 2040 after which they will start to decrease. OC emissions will also increase until 2040 and remain fairly constant until 2050. Emissions of VOC will increase from 2015 to 2050. NO$_x$ emissions will increase up to 2020 and remain fairly constant until 2030, after which they will decrease. SO$_2$ emissions are projected to decrease. The decrease from 2015 to 2020 will be stronger than from 2020 to 2050. The increase in the majority of the NTCF

emissions under SSP3-7.0 are estimated to mainly come from central Africa and southeast Asia and are associated with the continued reliance on fossil fuel sources for energy, transport and cooking needs (Gidden et al. 2019).

Under SSP3-7.0_lowNTCF, the emissions of CO, BC and OC remain constant until 2020 after which they start to decrease until 2050. The NO$_x$ emissions follow a similar trajectory, although they show a small decrease from 2015 to 2020. Emissions of VOC increase from 2015 to 2020 after which they decrease until 2050. Lastly, the SO$_2$ emissions will decrease sharply from 2015 to 2050. These NTCF emission reductions will be due to adoption of air pollution reduction policies.

Changes in PM$_{2.5}$

Figure 4 shows the projected changes in annual global average PM$_{2.5}$ from 2015 to 2055. Within the model framework, PM$_{2.5}$ is generated by the direct contribution of all fine aerosol varieties including nitrate, sulphate, carbonaceous, ammonium, dust and sea salt. The difference in PM$_{2.5}$ between SSP3-7.0 and SSP3-7.0_lowNTCF will be most apparent starting in 2045. That is when the mitigation efforts are estimated to start showing large benefits. Furthermore, as expected, NTCF mitigation will cause a significant decrease in PM$_{2.5}$ at a rate of
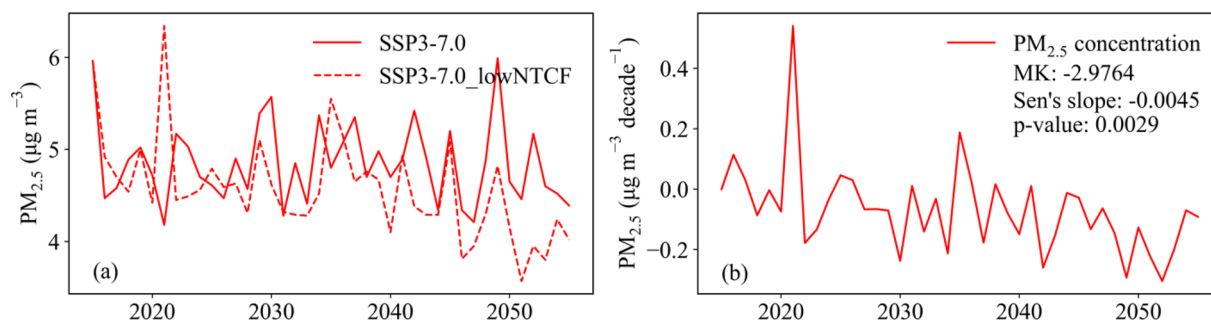
Fig. 4 **a** Projected changes in annual global average $PM_{2.5}$ concentration under SSP3-7.0 and SSP3-7.0_lowNTCF. **b** Projected changes due to NTCF mitigation. The plot includes the Mann–Kendall (MK) statistic and Sen's slope at a 95% confidence level

0.0045 $\mu g \ m^{-3} \ decade^{-1}$ over the 2015 to 2055 period and this expected to generate large benefits for air quality.

Downscaled temperature

Figure 5 shows the spatial trend of the projected mean surface temperature over the 2021 to 2055 period under annual, December–January–February (DJF), March–April–May (MAM), June–July–August (JJA) and September–October–November (SON) aggregations. Both SSP3-7.0 and SSP3-7.0_lowNTCF show significant warming across most of the region. This projected warming generally ranges from 0.001 to more than 0.015 °C $decade^{-1}$ and is associated with increasing CO_2 and CH_4 levels in both scenarios (Allen et al. 2020). A small but insignificant cooling is also projected during SON over Lake Malawi under SSP3-7.0.

The resultant NTCF mitigation signal shows warming in the majority of the region. The annual mean warming ranges between 0.005 and 0.01 °C $decade^{-1}$ and its mostly significant over parts of Kenya, Ethiopia, Somalia, and the Indian Ocean. DJF, MAM, JJA and SON have areas of both warming and cooling, although only the warming was significant. During MAM the warming intensifies to over 0.015 °C $decade^{-1}$ over southern Ethiopia and northern Tanzania. A similar warming trend happens during JJA over Ethiopia and Lake Victoria. During the same season, warming ranging between 0.005 and 0.01 °C $decade^{-1}$ occurs over the ocean. This projected warming due to NTCF mitigation results from global increase in the effective radiative forcing when aerosol loadings are reduced. Consequently, the cooling that comes from aerosol–radiation and aerosol–cloud interactions is reduced, and this causes the warming (Allen et al. 2020; Smith et al. 2020; Westervelt et al. 2015).

Surface temperature changes during DJF were not significant. Further, surface temperature was also averaged over selected countries to obtain time series of annual and seasonal aggregations for the 2021 to 2055 period (Fig. 6). When the Mann–Kendall test and Sen's slope

estimator were applied in this context, no trends were found (Table 2).

Downscaled precipitation

Figure 7 shows the trend of projected accumulated precipitation over the 2021 to 2055 period. Under SSP3-7.0, the region is dominated by a decrease in annual mean precipitation ranging between 0.1 and 0.5 mm $month^{-1} \ decade^{-1}$. This was most significant over the southern Kenya–northern Tanzania area and over the upper region of the Indian Ocean. This projected decrease is emphasized during JJA and SON. A significant precipitation decrease of about 0.5 mm $month^{-1} \ decade^{-1}$ is seen over South Sudan and the Indian Ocean during JJA and over large parts of Zambia, Tanzania, Kenya and Somalia during SON. During both seasons, a stronger precipitation decrease ranging from 0.7 to over 1.5 mm $month^{-1} \ decade^{-1}$ is seen over Lake Victoria and the coastal areas of Kenya and Tanzania. The DJF season differs from the other seasons, as it is dominated by precipitation increase ranging from 0.1 to over 1.5 mm $month^{-1} \ decade^{-1}$. This was significant over central Uganda and the Lake Victoria shores, northeastern Kenya, Somalia, parts of South Sudan and Ethiopia and parts of western and southern Tanzania.

Under SSP3-7.0_lowNTCF, the region is dominated by increase in annual mean precipitation. This is between 0.1 and 0.5 mm $month^{-1} \ decade^{-1}$ over Rwanda, northern Tanzania, southern and northern Uganda, west and central Kenya, parts of Ethiopia and South Sudan. The largest increase ranging from 1 to over 1.5 mm $month^{-1} \ decade^{-1}$ is over Lake Victoria and the southern shore of Tanzania that borders the Indian Ocean. A small decrease in annual mean precipitation is seen over Zambia, Malawi and southern Tanzania. This decrease ranges from 0.1 to 0.5 mm $month^{-1} \ decade^{-1}$. These precipitation changes are emphasized during different seasons. Precipitation increase over the southern coast of Tanzania is emphasized during DJF and MAM
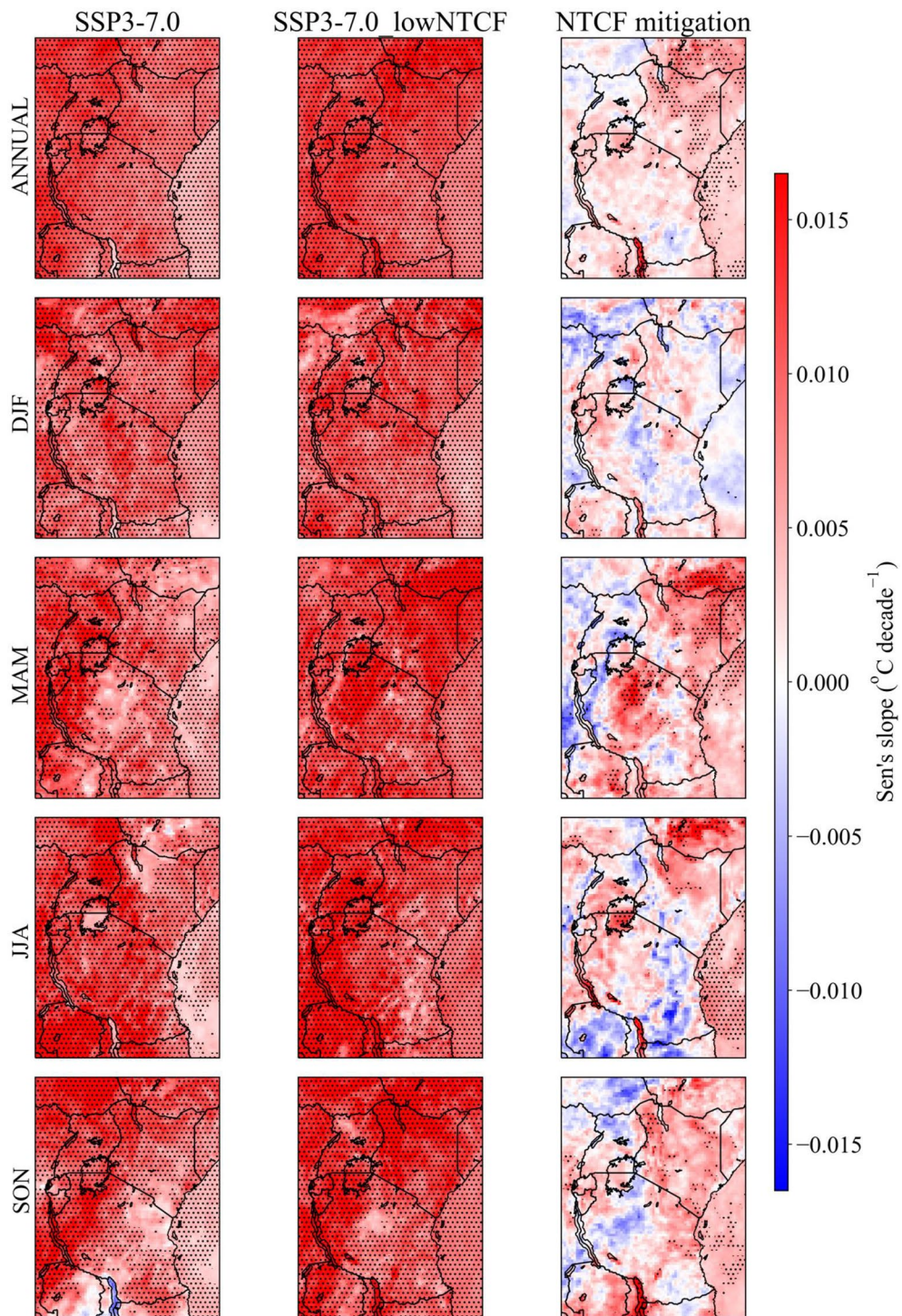
Fig. 5 Projected annual and seasonal mean surface temperature trend over the 2021 to 2055 period. Stippling denotes Mann–Kendall trend significance at the 95% confidence level

while the increase over Lake Victoria and the land areas is emphasized during MAM and SON. On the contrary, the precipitation decrease over the land areas is emphasized during SON, where large parts of Zambia, Malawi, southern Tanzania and northern Mozambique show a precipitation decrease of between 0.5 and
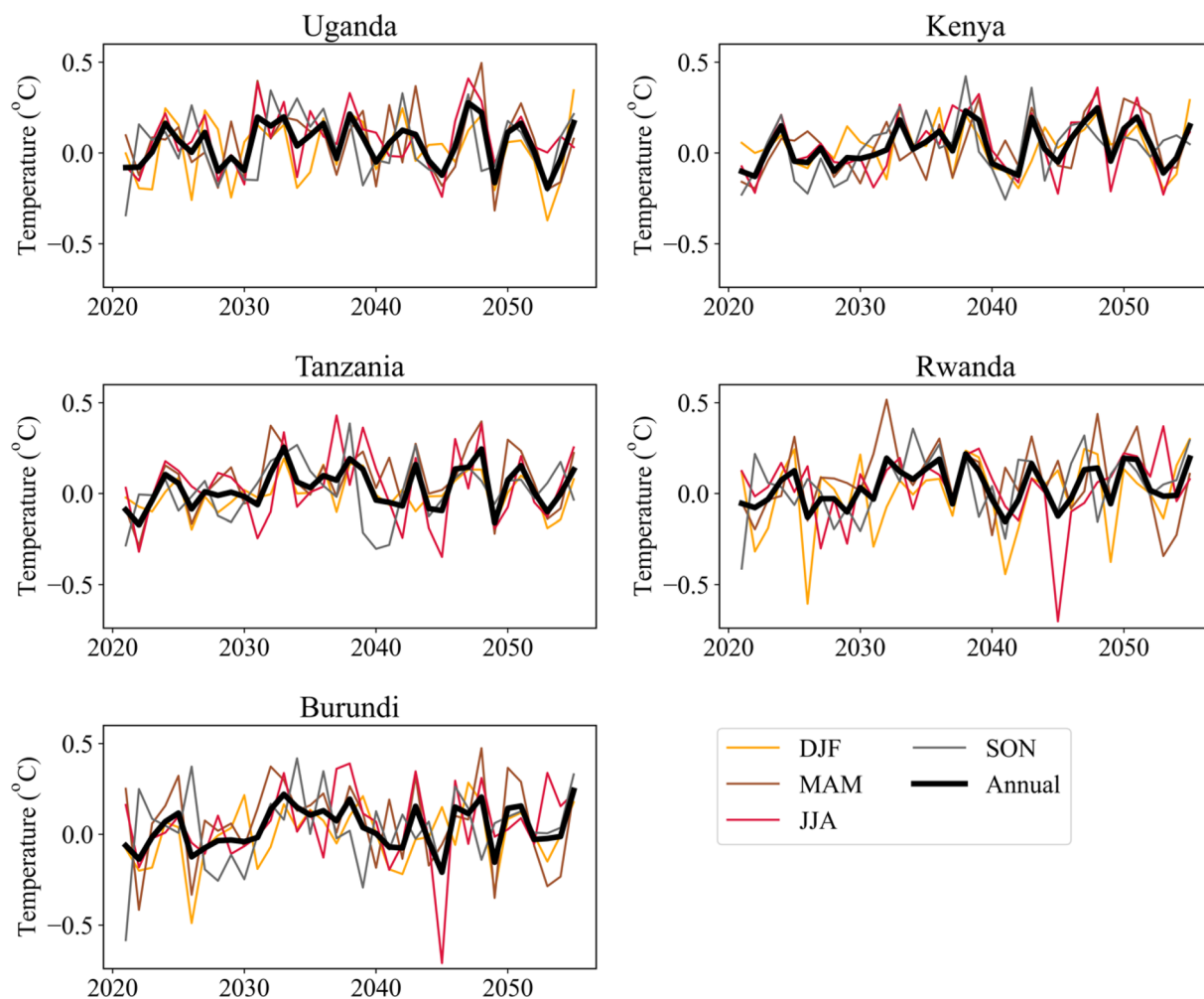
Fig. 6 Time series of area-averaged, projected surface temperature due to NTCF mitigation. The trend values are shown in Table 2

Table 2 Mann–Kendall test, standard normal statistic (Z) and Sen's slope (°C decade^{-1}) for surface temperature

	Annual	DJF	MAM	JJA	SON
Uganda	0.51/0.0013	0.11/0.0002	− 0.08/− 0.0001	0.62/0.0019	− 0.02/− 6.3211
Kenya	1.87/0.0037	0.45/0.0011	1.95/0.0053	0.88/0.0030	1.76/0.0044
Tanzania	1.07/0.0024	0.96/0.0018	1.59/0.0045	0.22/0.0009	0.79/0.0025
Rwanda	1.84/0.0025	1.05/0.0038	0.28/0.0009	0.34/0.0013	1.24/0.0040
Burundi	1.70/0.0033	1.39/0.0033	− 0.17/− 0.0012	1.30/0.0042	0.79/0.0024

The results are presented as Z/Sen's slope. There were no significant trends at the 95% confidence level

1 mm month^{-1} decade^{-1}. Precipitation decrease over the Indian Ocean is emphasized during JJA. There is also a precipitation increase over the ocean during MAM although not significant.

The resultant NTCF mitigation signal shows that the region is dominated by an increase in annual mean precipitation. This projected increase ranges from 0.1 to 1 mm month^{-1} decade^{-1} over northeastern Uganda, west and central Kenya, northern Tanzania and parts of South Sudan and Ethiopia. However, there is also a decrease in annual mean precipitation of up to 0.5 mm month^{-1} decade^{-1} in parts of Zambia, Malawi and southern Tanzania. This projected decrease in precipitation is emphasized during DJF, where it ranges
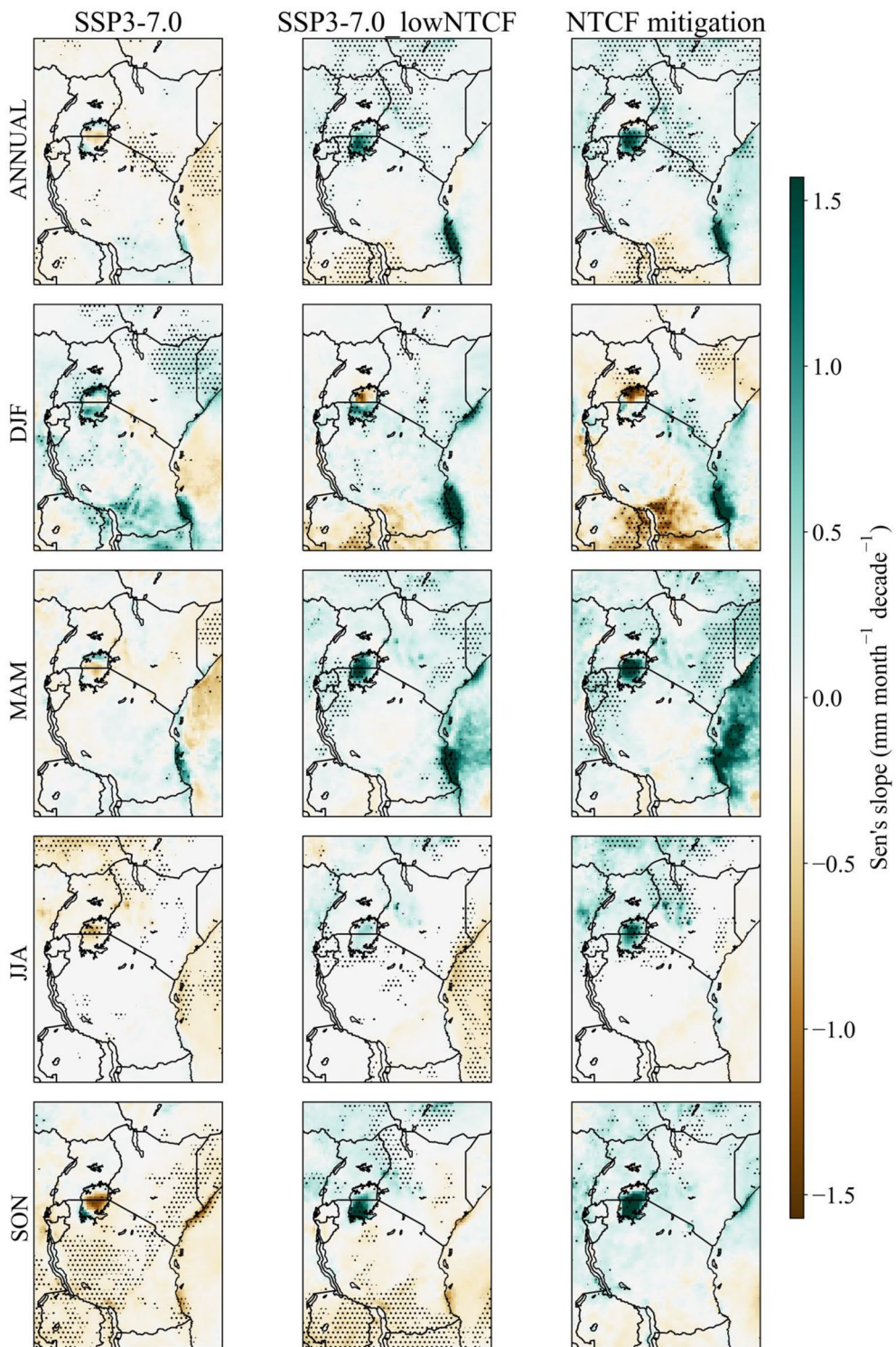
Fig. 7 Projected annual and seasonal trends in accumulated precipitation over the 2021 to 2055 period. Stippling denotes Mann–Kendall trend significance at the 95% confidence level
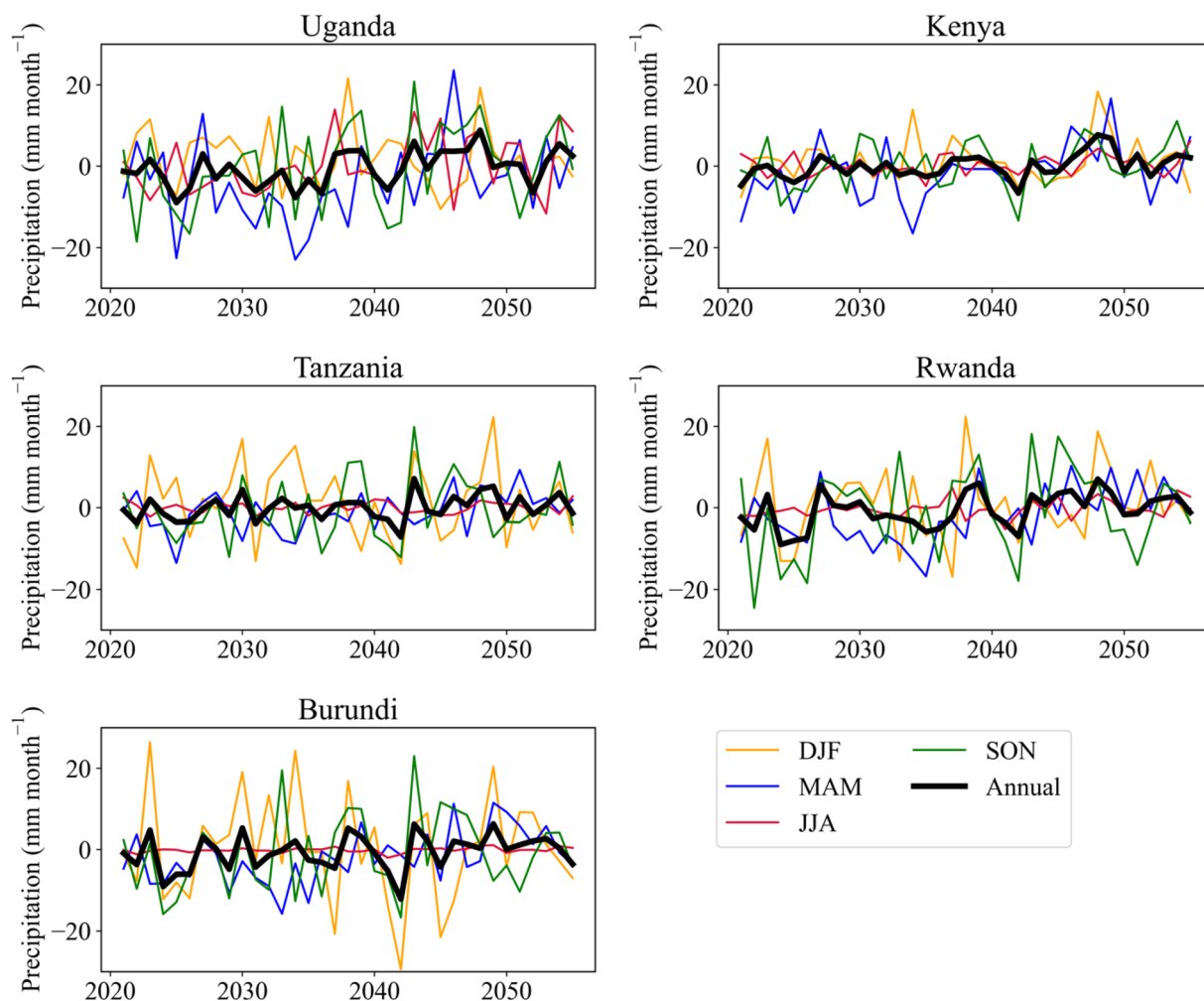
Fig. 8 Time series of area-averaged, projected accumulated precipitation due to NTCF mitigation. The trend values are shown in Table 3

from 0.5 to over 1.5 mm month^{-1} decade^{-1}. In the same season, other areas are seen to experience a precipitation decrease. These are central Uganda at about 0.5 mm month^{-1} decade^{-1}, the Lake Victoria shore at about 1.5 mm month^{-1} decade^{-1} and northeastern Kenya at about 0.5 mm month^{-1} decade^{-1}. There is also a small area in southern Kenya which has an increase in precipitation of up to 0.5 mm month^{-1} decade^{-1}.

The bulk of the precipitation increase is projected to happen during MAM and JJA. During MAM, it ranges from 0.1 to 1 mm month^{-1} decade^{-1} over Rwanda, Burundi, western Tanzania, northeastern Uganda, western Kenya and Somalia. In the same season, larger increases of over 1.5 mm month^{-1} decade^{-1} are seen over Lake Victoria, the upper coastal region of Kenya and Somalia, the southern coast of Tanzania and over the ocean. During JJA, the precipitation increase ranges from 0.1 to just over 1 mm month^{-1} decade^{-1} and is

mostly over western Kenya, Ethiopia and South Sudan. A stronger increase of about 1.5 mm month^{-1} decade^{-1} is also seen over Lake Victoria. The precipitation increase during SON is largely insignificant. Furthermore, the spatially averaged precipitation time series for selected countries were also obtained and tested for a trend (Fig. 8

Table 3 Mann–Kendall test, standard normal statistic (Z) and Sen's slope (mm month^{-1} decade^{-1}) for precipitation

	Annual	DJF	MAM	JJA	SON
Uganda	**2.44/0.196**	− 1.44/− 0.166	1.53/0.275	1.76/0.295	1.76/0.336
Kenya	**2.78/0.116**	− 0.08/− 0.005	**2.35/0.278**	1.27/0.056	1.50/0.163
Tanzania	1.70/0.075	− 0.19/− 0.027	1.87/0.163	0.19/0.008	0.88/0.078
Rwanda	**2.32/0.187**	0.11/0.032	**2.95/0.285**	1.70/0.059	0.68/0.172
Burundi	1.56/0.097	0.00/− 0.005	**2.44/0.265**	1.67/0.017	1.13/0.204

The results are presented as Z/Sen's slope. Significant trends at the 95% confidence level are denoted by bold font

Opio *et al. Environmental Systems Research*   (2023) 12:16

Page 12 of 16

and Table 3). An increasing precipitation trend occurs over Uganda, Kenya and Rwanda at rates of 0.196, 0.116 and 0.187 mm month^{-1} decade^{-1} respectively. Significant increments also occur during the MAM season over Kenya, Rwanda and Burundi at rates of 0.278, 0.285 and 0.265 mm month^{-1} decade^{-1} respectively.

The changes in aerosol–radiation and aerosol–cloud interactions also explain the increase and decrease in precipitation, although the stronger signal is the increase. This study aligns well with prior studies that show that aerosols have had and continue to have an important influence on East African precipitation (de Graaf et al. 2010; Mmame et al. 2023; Scannell et al. 2019). Further, this study has also shown that in addition to causing an increase and decrease in the precipitation over East Africa, NTCF mitigation will specifically cause the bulk of the precipitation increase during MAM. These results contradict Allen et al. (2020) who highlighted that NTCF mitigation only causes an increase in precipitation and mainly during DJF. This contradiction probably exists because the present study only downscaled one CMIP6 model and yet the results of Allen et al. (2020) are based on a multi-model ensemble of nine CMIP6 models. Furthermore, downscaling with WRF introduces additional biases and uncertainty to those already existing in the raw CMIP6 model output. Quantifying this model bias could help refine the results but it has not been addressed in the current scope of the study. Despite this, both studies agree on the increase in surface temperature.

Summary and conclusions

This study downscaled the MPI-ESM1-2-HAM global climate model output using the WRF regional climate model. Model experiments for two future scenarios, that is, one with weak air quality control (SSP3-7.0) and the other with strong air quality control (SSP3-7.0_lowNTCF) were downscaled from 250 to 23 km in order to study the local-scale projected climate change over East Africa due to global mitigation of NTCFs. This study concludes that global efforts to mitigate NTCFs could indeed improve air quality but it could also cause significant climate change in East Africa. Specifically, it could cause an increase in surface temperature in large parts of Kenya and some parts of Ethiopia and Somalia. It could also cause an increase in precipitation in several parts of the region, including Uganda, Kenya and Rwanda. Majority of the increase is projected to occur during the MAM season. On the other hand, parts of Zambia, Malawi and southern Tanzania could also experience a decrease in precipitation especially during the DJF season. Therefore, to avoid such a future in which air quality is improved but climate change worsened, it is recommended that both NTCFs and greenhouse gases be mitigated concurrently,

both locally and on a global scale. If such policies are used, it will help achieve a double benefit of improving air quality and combating climate change.

For further understanding of the possible climate change due to NTCF mitigation, future studies should be done using daily values of the meteorological variables. This will make the calculation of the climate change indices (Karl et al. 1999) possible. This was not possible in the present study because the assessments were based only on monthly values. If possible, future studies could also downscale model experiments that have all NTCFs including CH_4. Such results can be used to reveal the climate impact of CH_4 mitigation alone and/or the mitigation of all NTCFs plus CH_4. Since CH_4 has a positive radiative forcing, its mitigation could cause cooling which might offset the warming caused due to the mitigation of the other NTCFs. This kind of investigation was not possible in the present study because the MPI-ESM1-2-HAM model did not perform the experiment that included CH_4 mitigation. In addition, the results presented here are thought to have a level of bias but this was not quantified within the current scope of the study. Future studies could cover this as well. Lastly, in future, NTCF emission estimates will be improved and updated using new methodologies. This will help improve the model simulations and advance our understanding of the climate impact of NTCF mitigation.

Author contributions
RO: Conceptualization; data curation; formal analysis; investigation; methodology; software; validation; visualization; writing—original draft; writing—review and editing. IM: Methodology; supervision; writing—review and editing. JN-N: Supervision; writing—review and editing; project administration. AN: Conceptualization; Writing—review and editing. ITO: Writing—review and editing.

Availability of data and materials
The CMIP6 MPI-ESM1-2-HAM model data and emission inputs are freely available for download from the Earth System Grid Federation (ESFG) database that is hosted at the Lawrence Livermore National Laboratory. The downscaled WRF model output along with the analysis code have been deposited on GitHub at https://github.com/Opio-Cornelius/CMIP6_Downscaling_with_WRF.

Declarations

Ethics approval and consent to participate
Not applicable.

Opio *et al. Environmental Systems Research*   (2023) 12:16

Page 13 of 16

References

Aas W, Mortier A, Bowersox V, Cherian R, Faluvegi G, Fagerli H, Hand J, Klimont Z, Galy-Lacaux C, Lehmann CMB, Myhre CL, Myhre G, Olivié D, Sato K, Quaas J, Rao PSP, Schulz M, Shindell D, Skeie RB et al (2019) Global and regional trends of atmospheric sulfur. Sci Rep 9(1):1–11. https://doi.org/10.1038/s41598-018-37304-0

Akinsanola AA, Ongoma V, Kooperman GJ (2021) Evaluation of CMIP6 models in simulating the statistics of extreme precipitation over Eastern Africa. Atmos Res 254:105509. https://doi.org/10.1016/j.atmosres.2021.105509

Alemu H, Kaptué AT, Senay GB, Wimberly MC, Henebry GM (2015) Evapotranspiration in the Nile Basin: identifying dynamics and drivers, 2002–2011. Water (switzerland) 7(9):4914–4931. https://doi.org/10.3390/w7094914

Allen RJ, Turnock S, Nabat P, Neubauer D, Lohmann U, Olivié D, Oshima N, Michou M, Wu T, Zhang J, Takemura T, Schulz M, Tsigaridis K, Bauer SE, Emmons L, Horowitz L, Naik V, Van Noije T, Bergman T et al (2020) Climate and air quality impacts due to mitigation of non-methane near-term climate forcers. Atmos Chem Phys 20(16):9641–9663. https://doi.org/10.5194/ACP-20-9641-2020

Ayugi B, Ngoma H, Babaousmail H, Karim R, Iyakaremye V, Lim Kam Sian KTC, Ongoma V (2021) Evaluation and projection of mean surface temperature using CMIP6 models over East Africa. J Afr Earth Sci 181:104226. https://doi.org/10.1016/j.jafrearsci.2021.104226

Ayugi B, Jiang Z, Iyakaremye V, Ngoma H, Babaousmail H, Onyutha C, Dike VN, Mumo R, Ongoma V (2022a) East African population exposure to precipitation extremes under 15 °C and 20 °C warming levels based on CMIP6 models. Environ Res Lett 17(4):044051. https://doi.org/10.1088/1748-9326/ac5d9d

Ayugi B, Shilenje ZW, Babaousmail H, LimKamSian KTC, Mumo R, Dike VN, Iyakaremye V, Chehbouni A, Ongoma V (2022b) Projected changes in meteorological drought over East Africa inferred from bias-adjusted CMIP6 models. Nat Hazards 113(2):1151–1176. https://doi.org/10.1007/S11069-022-05341-8/FIGURES/1

Baker LH, Collins WJ, Olivié DJL, Cherian R, Hodnebrog, Myhre G, Quaas J (2015) Climate responses to anthropogenic emissions of short-lived climate pollutants. Atmos Chem Phys 15(14):8201–8216. https://doi.org/10.5194/acp-15-8201-2015

Baño-Medina J, Manzanas R, Gutierrez JM (2020) Configuration and intercomparison of deep learning neural models for statistical downscaling. Geosci Model Dev 13(4):2109–2124. https://doi.org/10.5194/gmd-13-2109-2020

Buchholz RR, Worden HM, Park M, Francis G, Deeter MN, Edwards DP, Emmons LK, Gaubert B, Gille J, Martínez-Alonso S, Tang W, Kumar R, Drummond JR, Clerbaux C, George M, Coheur PF, Hurtmans D, Bowman KW, Luo M et al (2021) Air pollution trends measured from Terra: CO and AOD over industrial, fire-prone, and background regions. Remote Sens Environ 256:112275. https://doi.org/10.1016/J.RSE.2020.112275

Chen F, Dudhia J (2001) Coupling an advanced land surface-hydrology model with the Penn State–NCAR MM5 Modeling System. Part I: model implementation and sensitivity. Mon Weather Rev. https://doi.org/10.1175/1520-0493(2001)129%3c0569:CAALSH%3e2.0.CO;2

Cohen AJ, Brauer M, Burnett R, Anderson HR, Frostad J, Estep K, Balakrishnan K, Brunekreef B, Dandona L, Dandona R, Feigin V, Freedman G, Hubbell B, Jobling A, Kan H, Knibbs L, Liu Y, Martin R, Morawska L et al (2017) Estimates and 25-year trends of the global burden of disease attributable to ambient air pollution: an analysis of data from the Global Burden of Diseases Study 2015. The Lancet 389(10082):1907–1918. https://doi.org/10.1016/S0140-6736(17)30505-6

Collins JW, Lamarque JF, Schulz M, Boucher O, Eyring V, Hegglin IM, Maycock A, Myhre G, Prather M, Shindell D, Smith JS (2017) AerChemMIP: quantifying the effects of chemistry and aerosols in CMIP6. Geosci Model Dev 10(2):585–607. https://doi.org/10.5194/gmd-10-585-2017

de Graaf M, Tilstra LG, Aben I, Stammes P (2010) Satellite observations of the seasonal cycles of absorbing aerosols in Africa related to the monsoon rainfall, 1995–2008. Atmos Environ 44(10):1274–1283. https://doi.org/10.1016/J.ATMOSENV.2009.12.038

Di Luca A, de Elía R, Laprise R (2012) Potential for added value in precipitation simulated by high-resolution nested Regional Climate Models and observations. Clim Dyn 38(5–6):1229–1247. https://doi.org/10.1007/S00382-011-1068-3/FIGURES/10

Di Luca A, de Elía R, Laprise R (2015) Challenges in the quest for added value of regional climate dynamical downscaling. Curr Clim Change Rep 1(1):10–21. https://doi.org/10.1007/S40641-015-0003-9/FIGURES/2

Dunne JP, Horowitz LW, Adcroft AJ, Ginoux P, Held IM, John JG, Krasting JP, Malyshev S, Naik V, Paulot F, Shevliakova E, Stock CA, Zadeh N, Balaji V, Blanton C, Dunne KA, Dupuis C, Durachta J, Dussin R et al (2020) The GFDL Earth System Model Version 4.1 (GFDL-ESM 4.1): overall coupled model description and simulation characteristics. J Adv Model Earth Syst 12(11):e2019MS002015. https://doi.org/10.1029/2019MS002015

Emmons LK, Schwantes RH, Orlando JJ, Tyndall G, Kinnison D, Lamarque JF, Marsh D, Mills MJ, Tilmes S, Bardeen C, Buchholz RR, Conley A, Gettelman A, Garcia R, Simpson I, Blake DR, Meinardi S, Pétron G (2020) The chemistry mechanism in the community earth system model version 2 (CESM2). J Adv Model Earth Syst 12(4):e2019MS001882. https://doi.org/10.1029/2019MS001882

Fernández-Alvarez JC, Costoya X, Pérez-Alarcón A, Rahimi S, Nieto R, Gimeno L (2023) Dynamic downscaling of wind speed over the North Atlantic Ocean using CMIP6 projections: implications for offshore wind power density. Energy Rep 9:873–885. https://doi.org/10.1016/J.EGYR.2022.12.036

Finney DL, Marsham JH, Walker DP, Birch CE, Woodhams BJ, Jackson LS, Hardy S (2020) The effect of westerlies on East African rainfall and the associated role of tropical cyclones and the Madden–Julian Oscillation. Q J R Meteorol Soc 146(727):647–664. https://doi.org/10.1002/qj.3698

Fowler D, Brimblecombe P, Burrows J, Heal MR, Grennfelt P, Stevenson DS, Jowett A, Nemitz E, Coyle M, Lui X, Chang Y, Fuller GW, Sutton MA, Klimont Z, Unsworth MH, Vieno M (2020) A chronology of global air quality: the development of global air pollution. Philos Trans R Soc A Math Phys Eng Sci 378(2183):20190314. https://doi.org/10.1098/rsta.2019.0314

Fujimori S, Hasegawa T, Masui T, Takahashi K, Herran DS, Dai H, Hijioka Y, Kainuma M (2017) SSP3: AIM implementation of shared socioeconomic pathways. Glob Environ Chang 42:268–283. https://doi.org/10.1016/J.GLOENVCHA.2016.06.009

Gebrechorkos SH, Hülsmann S, Bernhofer C (2019a) Long-term trends in rainfall and temperature using high-resolution climate datasets in East Africa. Sci Rep 9(1):1–9. https://doi.org/10.1038/s41598-019-47933-8

Gebrechorkos SH, Hülsmann S, Bernhofer C (2019b) Changes in temperature and precipitation extremes in Ethiopia, Kenya, and Tanzania. Int J Climatol 39(1):18–30. https://doi.org/10.1002/JOC.5777

Gettelman A, Mills MJ, Kinnison DE, Garcia RR, Smith AK, Marsh DR, Tilmes S, Vitt F, Bardeen CG, McInerny J, Liu HL, Solomon SC, Polvani LM, Emmons LK, Lamarque JF, Richter JH, Glanville AS, Bacmeister JT, Phillips AS et al (2019) The whole atmosphere community climate model version 6 (WACCM6). J Geophys Res Atmos 124(23):12380–12403. https://doi.org/10.1029/2019JD030943

Gidden M, Riahi K, Smith S, Fujimori S, Luderer G, Kriegler E, van Vuuren D, van den Berg M, Feng L, Klein D, Calvin K, Doelman J, Frank S, Fricko O, Harmsen M, Hasegawa T, Havlik P, Hilaire J, Hoesly R, et al (2018a) input4MIPs. CMIP6.AerChemMIP.IAMC.IAMC-AIM-ssp370-lowNTCF-1-1. Earth system grid federation. https://doi.org/10.22033/ESGF/input4MIPs.2481

Gidden M, Riahi K, Smith S, Fujimori S, Luderer G, Kriegler E, van Vuuren D, van den Berg M, Feng L, Klein D, Calvin K, Doelman J, Frank S, Fricko O, Harmsen M, Hasegawa T, Havlik P, Hilaire J, Hoesly R, Takahashi K (2018b) input4MIPs.CMIP6.ScenarioMIP.IAMC.IAMC-AIM-ssp370-1-1. Earth system grid federation. https://doi.org/10.22033/ESGF/input4MIPs.2482

Gidden M, Riahi K, Smith SJ, Fujimori S, Luderer G, Kriegler E, Van Vuuren DP, Van Den Berg M, Feng L, Klein D, Calvin K, Doelman JC, Frank S, Fricko O, Harmsen M, Hasegawa T, Havlik P, Hilaire J, Hoesly R et al (2019) Global emissions pathways under different socioeconomic scenarios for use in CMIP6: a dataset of harmonized emissions trajectories through the end of

Opio *et al. Environmental Systems Research*   (2023) 12:16

Page 14 of 16

the century. Geosci Model Dev 12(4):1443–1475. https://doi.org/10.5194/gmd-12-1443-2019

Giorgi F, Gutowski WJ (2015) Regional dynamical downscaling and the CORDEX initiative. 40:467–490. https://doi.org/10.1146/ANNUREV-ENVIRON-102014-021217

Gocic M, Trajkovic S (2013) Analysis of changes in meteorological variables using Mann-Kendall and Sen's slope estimator statistical tests in Serbia. Glob Planet Change. https://doi.org/10.1016/j.gloplacha.2012.10.014

Gomez J, Allen RJ, Turnock ST, Horowitz LW, Tsigaridis K, Bauer SE, Olivié D, Thomson ES, Ginoux P (2023) The projected future degradation in air quality is caused by more abundant natural aerosols in a warmer world. Commun Earth Environ 4(1):22. https://doi.org/10.1038/s43247-023-00688-7

Grell GA, Dévényi D (2002) A generalized approach to parameterizing convection combining ensemble and data assimilation techniques. Geophys Res Lett 29(14):10–13. https://doi.org/10.1029/2002GL015311

Hassan T, Allen RJ, Liu W, Shim S, van Noije T, Le Sager P, Oshima N, Deushi M, Randles CA, O'Connor FM (2022) Air quality improvements are projected to weaken the Atlantic meridional overturning circulation through radiative forcing effects. Commun Earth Environ 3(1):1–12. https://doi.org/10.1038/s43247-022-00476-9

Hoesly RM, Smith SJ, Feng L, Klimont Z, Janssens-Maenhout G, Pitkanen T, Seibert JJ, Vu L, Andres RJ, Bolt RM, Bond TC, Dawidowski L, Kholod N, Kurokawa JI, Li M, Liu L, Lu Z, Moura MCP, O'Rourke PR, Zhang Q (2018) Historical (1750–2014) anthropogenic emissions of reactive gases and aerosols from the Community Emissions Data System (CEDS). Geosci Model Dev 11(1):369–408. https://doi.org/10.5194/GMD-11-369-2018

Hong S-Y, Noh Y, Dudhia J (2006) A new vertical diffusion package with an explicit treatment of entrainment processes. Mon Weather Rev. https://doi.org/10.1175/MWR3199.1

Horowitz LW, Naik V, Paulot F, Ginoux PA, Dunne JP, Mao J, Schnell J, Chen X, He J, John JG, Lin M, Lin P, Malyshev S, Paynter D, Shevliakova E, Zhao M (2020) The GFDL global atmospheric chemistry-climate model AM4.1: model description and simulation characteristics. J Adv Model Earth Syst 12(10):2019MS002032. https://doi.org/10.1029/2019MS002032

Iacono MJ, Delamere JS, Mlawer EJ, Shephard MW, Clough SA, Collins WD (2008) Radiative forcing by long-lived greenhouse gases: calculations with the AER radiative transfer models. J Geophys Res Atmos 113(13):2–9. https://doi.org/10.1029/2008JD009944

Jacob DJ (2021) Introduction to atmospheric chemistry: supplemental questions and problems, 11th ed, Harvard University. https://projects.iq.harvard.edu/files/acmg/files/edu_jacob_atmchem_problems_jan_2021.pdf

Jiang Z, McDonald BC, Worden H, Worden JR, Miyazaki K, Qu Z, Henze DK, Jones DBA, Arellano AF, Fischer EV, Zhu L, Folkert Boersma K (2018) Unexpected slowdown of US pollutant emission reduction in the past decade. Proc Natl Acad Sci USA 115(20):5099–5104. https://doi.org/10.1073/PNAS.1801191115/SUPPL_FILE/PNAS.1801191115.SAPP.PDF

Karl TR, Nicholls N, Ghazi A (1999) CLIVAR/GCOS/WMO workshop on indices and indicators for climate extremes—workshop summary. Clim Change. https://doi.org/10.1023/A:1005491526870

Kasoar M, Voulgarakis A, Lamarque JF, Shindell DT, Bellouin N, Collins WJ, Faluvegi G, Tsigaridis K (2016) Regional and global temperature response to anthropogenic SO2 emissions from China in three climate models. Atmos Chem Phys 16(15):9785–9804. https://doi.org/10.5194/acp-16-9785-2016

Kendall MG (1975) Rank correlation methods, 4th edn. Charles Griffin, San Francisco

Lelieveld J, Klingmüller K, Pozzer A, Burnett RT, Haines A, Ramanathan V (2019) Effects of fossil fuel and total anthropogenic emission removal on public health and climate. Proc Natl Acad Sci USA 116(15):7192–7197. https://doi.org/10.1073/pnas.1819989116

Li J, Deng S, Li G, Lu Z, Song H, Gao J, Sun Z, Xu K (2022) VOCs characteristics and their ozone and SOA formation potentials in autumn and winter at Weinan, China. Environ Res 203:111821. https://doi.org/10.1016/j.envres.2021.111821

Lin Y-L, Farley RD, Orville HD (1983) Bulk parameterization of the snow field in a cloud model. J Appl Meteorol Climatol. https://doi.org/10.1175/1520-0450(1983)022%3c1065:BPOTSF%3e2.0.CO;2

Lu H, Lyu X, Cheng H, Ling Z, Guo H (2019) Overview on the spatial-temporal characteristics of the ozone formation regime in China. Environ Sci Process Impacts 21(6):916–929. https://doi.org/10.1039/c9em00098d

Makula EK, Zhou B (2022) Coupled Model Intercomparison Project phase 6 evaluation and projection of East African precipitation. Int J Climatol 42(4):2398–2412. https://doi.org/10.1002/joc.7373

Mann HB (1945) Nonparametric tests against trend. Econometrica 13(3):245–259

Mauritsen T, Bader J, Becker T, Behrens J, Bittner M, Brokopf R, Brovkin V, Claussen M, Crueger T, Esch M, Fast I, Fiedler S, Fläschner D, Gayler V, Giorgetta M, Goll DS, Haak H, Hagemann S, Hedemann C et al (2019) Developments in the MPI-M Earth System Model version 12 (MPI-ESM12) and its response to increasing CO2. J Adv Model Earth Syst 11(4):998–1038. https://doi.org/10.1029/2018MS001400

Michou M, Nabat P, Saint-Martin D, Bock J, Decharme B, Mallet M, Roehrig R, Séférian R, Sénési S, Voldoire A (2020) Present-day and historical aerosol and ozone characteristics in CNRM CMIP6 simulations. J Adv Model Earth Syst 12(1):2019MS001816. https://doi.org/10.1029/2019MS001816

Miller MR, Newby DE (2020) Air pollution and cardiovascular disease: car sick. Cardiovasc Res 116(2):279–294. https://doi.org/10.1093/cvr/cvz228

Miyazaki K, Eskes H, Sudo K, Folkert Boersma K, Bowman K, Kanaya Y (2017) Decadal changes in global surface NOx emissions from multi-constituent satellite data assimilation. Atmos Chem Phys 17(2):807–837. https://doi.org/10.5194/ACP-17-807-2017

Mmame B, Sunitha P, Samatha K (2023) Identification of sources and sinks of atmospheric aerosols and their impact on east African rainfall. Acta Geophys. https://doi.org/10.1007/S11600-023-01022-7/METRICS

Mölg T, Pickler C (2022) A mid-troposphere perspective on the East African climate paradox. Environ Res Lett 17(8):084041. https://doi.org/10.1088/1748-9326/ac8565

Muthoni FK, Odongo VO, Ochieng J, Mugalavai EM, Mourice SK, Hoesche-Zeledon I, Mwila M, Bekunda M (2019) Long-term spatial-temporal trends and variability of rainfall over Eastern and Southern Africa. Theor Appl Climatol 137(3–4):1869–1882. https://doi.org/10.1007/s00704-018-2712-1

Neubauer D, Ferrachat S, Siegenthaler-Le Drian C, Stoll J, Folini DS, Tegen I, Wieners K-H, Mauritsen T, Stemmler I, Barthel S, Bey I, Daskalakis N, Heinold B, Kokkola H, Partridge D, Rast S, Schmidt H, Schutgens N, Stanelle T, et al (2019) HAMMOZ-Consortium MPI-ESM1.2-HAM model output prepared for CMIP6 AerChemMIP. In: Earth System Grid Federation. Earth System Grid Federation. https://doi.org/10.22033/ESGF/CMIP6.1621

Ngoma H, Wen W, Ojara M, Ayugi B (2021) Assessing current and future spatiotemporal precipitation variability and trends over Uganda, East Africa, based on CHIRPS and regional climate model datasets. Meteorol Atmos Phys 133(3):823–843. https://doi.org/10.1007/S00703-021-00784-3/METRICS

Nicholson SE (2017) Climate and climatic variability of rainfall over eastern Africa. Rev Geophys 55(3):590–635. https://doi.org/10.1002/2016RG000544

Nicholson SE (2019). a review of climate dynamics and climate variability in Eastern Africa. In: The limnology, climatology and paleoclimatology of the East African lakes, Routledge, pp 25–56. https://doi.org/10.1201/9780203748978-2

Nooni IK, Tan G, Hongming Y, Saidou Chaibou AA, Habtemicheal BA, Gnitou GT, Lim KamSian KTC (2022) Assessing the performance of WRF model in simulating heavy precipitation events over east africa using satellite-based precipitation product. Remote Sens 14(9):1964. https://doi.org/10.3390/rs14091964

O'Neill BC, Tebaldi C, Van Vuuren DP, Eyring V, Friedlingstein P, Hurtt G, Knutti R, Kriegler E, Lamarque J, Lowe J, Meehl GA, Moss R, Riahi K, Sanderson BM (2016) The Scenario Model Intercomparison Project (ScenarioMIP) for CMIP6. Geosci Model Dev. https://doi.org/10.5194/gmd-9-3461-2016

Onyutha C (2016) Identification of sub-trends from hydro-meteorological series. Stoch Environ Res Risk Assess 30(1):189–205. https://doi.org/10.1007/s00477-015-1070-0

Otieno G, Mutemi JN, Opijah FJ, Ogallo LA, Omondi MH (2019) The sensitivity of rainfall characteristics to cumulus parameterization schemes from a WRF model. Part I: a case study over east africa during wet years. Pure Appl Geophys 177(2):1095–1110. https://doi.org/10.1007/S00024-019-02293-2

Pozzer A, Anenberg SC, Dey S, Haines A, Lelieveld J, Chowdhury S (2023) Mortality attributable to ambient air pollution: a review of global estimates. GeoHealth 7(1):e2022GH000711. https://doi.org/10.1029/2022GH000711

Rahimi S, Krantz W, Bass BJ, Goldenson NL, Hall AD, Lebo ZJ, Rahimi S, Krantz W, Bass BJ, Goldenson NL, Hall AD, Lebo ZJ (2020) Multi-resolution

Opio *et al. Environmental Systems Research*   (2023) 12:16

Page 15 of 16

dynamical downscaling of CMIP6 GCMs across the Western United States using WRF4: quantifying climate change uncertainty down to the convective scale. American Geophysical Union, Fall Meeting 2020, 2020, A093-0018. https://ui.adsabs.harvard.edu/abs/2020AGUFMA093.0018R/abstract

Samset BH, Sand M, Smith CJ, Bauer SE, Forster PM, Fuglestvedt JS, Osprey S, Schleussner CF (2018) Climate impacts from a removal of anthropogenic aerosol emissions. Geophys Res Lett 45(2):1020–1029. https://doi.org/10.1002/2017GL076079

Scannell C, Booth BBB, Dunstone NJ, Rowell DP, Bernie DJ, Kasoar M, Voulgarakis A, Wilcox LJ, Acosta Navarro JC, Seland Ø, Paynter DJ (2019) The influence of remote aerosol forcing from industrialized economies on the future evolution of East and West African rainfall. J Clim 32(23):8335–8354. https://doi.org/10.1175/JCLI-D-18-0716.1

Séférian R, Nabat P, Michou M, Saint-Martin D, Voldoire A, Colin J, Decharme B, Delire C, Berthet S, Chevallier M, Sénési S, Franchisteguy L, Vial J, Mallet M, Joetzjer E, Geoffroy O, Guérémy JF, Moine MP, Msadek R et al (2019) Evaluation of CNRM earth system model, CNRM-ESM2-1: role of earth system processes in present-day and future climate. J Adv Model Earth Syst 11(12):4182–4227. https://doi.org/10.1029/2019MS001791

Seland Ø, Bentsen M, Olivié D, Toniazzo T, Gjermundsen A, Graff LS, Debernard JB, Gupta AK, He YC, Kirkevåg A, Schwinger J, Tjiputra J, Schanke Aas K, Bethke I, Fan Y, Griesfeller J, Grini A, Guo C, Ilicak M et al (2020) Overview of the Norwegian Earth System Model (NorESM2) and key climate response of CMIP6 DECK, historical, and scenario simulations. Geosci Model Dev 13(12):6165–6200. https://doi.org/10.5194/GMD-13-6165-2020

Sellar AA, Jones CG, Mulcahy JP, Tang Y, Yool A, Wiltshire A, O'Connor FM, Stringer M, Hill R, Palmieri J, Woodward S, de Mora L, Kuhlbrodt T, Rumbold ST, Kelley DI, Ellis R, Johnson CE, Walton J, Abraham NL et al (2019) UKESM1: description and evaluation of the U.K. earth system model. J Adv Model Earth Syst 11(12):4513–4558. https://doi.org/10.1029/2019MS001739

Sen PK (1968) Estimates of the regression coefficient based on Kendall's Tau. J Am Stat Assoc 63(324):1379–1389. https://doi.org/10.1080/01621459.1968.10480934

Skamarock WC, Klemp JB, Dudhia J, Gill DO, Zhiquan L, Berner J, Wang W, Powers JG, Duda MG, Barker DM, Huang X-Y (2019) A description of the advanced research WRF Model Version 4. In: NCAR technical note NCAR/TN-556+STR. https://doi.org/10.5065/1dfh-6p97

Smith CJ, Kramer RJ, Myhre G, Alterskjr K, Collins W, Sima A, Boucher O, Dufresne JL, Nabat P, Michou M, Yukimoto S, Cole J, Paynter D, Shiogama H, O'Connor FM, Robertson E, Wiltshire A, Andrews T, Hannay C et al (2020) Effective radiative forcing and adjustments in CMIP6 models. Atmos Chem Phys 20(16):9591–9618. https://doi.org/10.5194/ACP-20-9591-2020

Szopa S, Naik V, Adhikary B, Artaxo P, Berntsen T, Collins WD, Fuzzi S, Gallardo L, Kiendler Scharr A, Klimont Z, Liao H, Unger N, Zanis P (2021) Short-lived climate forcers. In: Climate change 2021: the physical science basis. Contribution of working group I to the sixth assessment report of the intergovernmental panel on climate change, pp 817–922. https://doi.org/10.1017/9781009157896.008

Takemura T, Nozawa T, Emori S, Nakajima TY, Nakajima T (2005) Simulation of climate response to aerosol direct and indirect effects with aerosol transport-radiation model. J Geophys Res Atmos 110(D2):1–16. https://doi.org/10.1029/2004JD005029

Takemura T, Egashira M, Matsuzawa K, Ichijo H, O'Ishi R, Abe-Ouchi A (2009) A simulation of the global distribution and radiative forcing of soil dust aerosols at the Last Glacial Maximum. Atmos Chem Phys 9(9):3061–3073. https://doi.org/10.5194/ACP-9-3061-2009

Tatebe H, Ogura T, Nitta T, Komuro Y, Ogochi K, Takemura T, Sudo K, Sekiguchi M, Abe M, Saito F, Chikira M, Watanabe S, Mori M, Hirota N, Kawatani Y, Mochizuki T, Yoshimura K, Takata K, O'Ishi R et al (2019) Description and basic evaluation of simulated mean state, internal variability, and climate sensitivity in MIROC6. Geosci Model Dev 12(7):2727–2765. https://doi.org/10.5194/GMD-12-2727-2019

Tegen I, Neubauer D, Ferrachat S, Le Drian CS, Bey I, Schutgens N, Stier P, Watson-Parris D, Stanelle T, Schmidt H, Rast S, Kokkola H, Schultz M, Schroeder S, Daskalakis N, Barthel S, Heinold B, Lohmann U (2019) The global aerosol-climate model echam6.3-ham2.3—Part 1: aerosol

evaluation. Geosci Model Dev 12(4):1643–1677. https://doi.org/10.5194/GMD-12-1643-2019

Thrasher B, Wang W, Michaelis A, Melton F, Lee T, Nemani R (2022) NASA global daily downscaled projections, CMIP6. Sci Data 9(1):262. https://doi.org/10.1038/s41597-022-01393-4

Tilmes S, Hodzic A, Emmons LK, Mills MJ, Gettelman A, Kinnison DE, Park M, Lamarque JF, Vitt F, Shrivastava M, Campuzano-Jost P, Jimenez JL, Liu X (2019) Climate forcing and trends of organic aerosols in the community earth system model (CESM2). J Adv Model Earth Syst 11(12):4323–4351. https://doi.org/10.1029/2019MS001827

Vashisht A, Zaitchik B, Vashisht A, Zaitchik B (2021) MJO teleconnections over East Africa in general circulation models: a study of the recent past and the future. AGU fall meeting, 2021, A55U-1718. https://ui.adsabs.harvard.edu/abs/2021AGUFM.A55U1718V/abstract

Wainwright CM, Marsham JH, Keane RJ, Rowell DP, Finney DL, Black E, Allan RP (2019) 'Eastern African Paradox' rainfall decline due to shorter not less intense Long Rains. NPJ Clim Atmos Sci. https://doi.org/10.1038/s41612-019-0091-7

Walker DP, Marsham JH, Birch CE, Scaife AA, Finney DL (2020) Common mechanism for interannual and decadal variability in the East African long rains. Geophys Res Lett 47(22):e2020GL089182. https://doi.org/10.1029/2020GL089182

Walton DB, Sun F, Hall A, Capps S (2015) A hybrid dynamical-statistical downscaling technique. Part I: Development and validation of the technique. J Clim 28(12):4597–4617. https://doi.org/10.1175/JCLI-D-14-00196.1

Wenhaji Ndomeni C, Cattani E, Merino A, Levizzani V (2018) An observational study of the variability of East African rainfall with respect to sea surface temperature and soil moisture. Q J R Meteorol Soc 144:384–404. https://doi.org/10.1002/QJ.3255

Westervelt DM, Horowitz LW, Naik V, Golaz JC, Mauzerall DL (2015) Radiative forcing and climate response to projected 21st century aerosol decreases. Atmos Chem Phys 15(22):12681–12703. https://doi.org/10.5194/ACP-15-12681-2015

Willmott CJ, Ackleson SG, Davis RE, Feddema JJ, Klink KM, Legates DR, O'donnell J, Rowe C (1985) Statistics for the evaluation and comparison of models. J Geophys Res 90(5):8995–9005. https://doi.org/10.1029/JC090iC05p08995

World Health Organization (2018) Burden of disease from ambient air pollution for 2016. https://www.who.int/airpollution/data/AAP_BoD_results_May2018_final.pdf

Wu T, Lu Y, Fang Y, Xin X, Li L, Li W, Jie W, Zhang J, Liu Y, Zhang L, Zhang F, Zhang Y, Wu F, Li J, Chu M, Wang Z, Shi X, Liu X, Wei M et al (2019) The Beijing Climate Center Climate System Model (BCC-CSM): the main progress from CMIP5 to CMIP6. Geosci Model Dev 12(4):1573–1600. https://doi.org/10.5194/GMD-12-1573-2019

Wu T, Zhang F, Zhang J, Jie W, Zhang Y, Wu F, Li L, Yan J, Liu X, Lu X, Tan H, Zhang L, Wang J, Hu A (2020) Beijing Climate Center Earth System Model version 1 (BCC-ESM1): model description and evaluation of aerosol simulations. Geosci Model Dev 13(3):977–1005. https://doi.org/10.5194/GMD-13-977-2020

Xu Z, Han Y, Yang Z (2019) Dynamical downscaling of regional climate: a review of methods and limitations. Sci China Earth Sci 62(2):365–375. https://doi.org/10.1007/S11430-018-9261-5/METRICS

Xu Z (2021) A bias-corrected CMIP6 dataset and its application and validation in dynamical downscaling simulation of Asia. AGU fall meeting 2021, 2021, GC35K-0806. https://ui.adsabs.harvard.edu/abs/2021AGUFMGC35K0806X/abstract

Yang X, Li D, Yang Z, Wu K, Ji L, Zhou Z, Lu Y (2023) Revealing historical observations and future projections of precipitation over Northwest China based on dynamic downscaled CMIP6 simulations. Front Earth Sci 10:2316. https://doi.org/10.3389/FEART.2022.1090221/BIBTEX

Ye Z, Im U, Christensen J, Geels C, Sandstad M, Iles C, Schwingshackl C (2022) Near-past and future trends of European extreme heat and heat waves from WRF downscaling experiments. EGU22. https://doi.org/10.5194/EGUSPHERE-EGU22-11296

Yu E, Liu D, Yang J, Sun J, Yu L, King MP (2023) Future climate change for major agricultural zones in China as projected by CORDEX-EA-II, CMIP5 and CMIP6 ensembles. Atmos Res 288:106731. https://doi.org/10.1016/J.ATMOSRES.2023.106731

Yukimoto S, Kawai H, Koshiro T, Oshima N, Yoshida K, Urakawa S, Tsujino H, Deushi M, Tanaka T, Hosaka M, Yabu S, Yoshimura H, Shindo E, Mizuta R,

Opio *et al. Environmental Systems Research*   (2023) 12:16

Page 16 of 16

Obata A, Adachi Y, Ishii M (2019) The meteorological research institute Earth system model version 2.0, MRI-ESM20: description and basic evaluation of the physical component. J Meteorol Soc Jpn 97(5):931–965. https://doi.org/10.2151/jmsj.2019-051

Zheng B, Tong D, Li M, Liu F, Hong C, Geng G, Li H, Li X, Peng L, Qi J, Yan L, Zhang Y, Zhao H, Zheng Y, He K, Zhang Q (2018) Trends in China's anthropogenic emissions since 2010 as the consequence of clean air actions. Atmos Chem Phys 18(19):14095–14111. https://doi.org/10.5194/ACP-18-14095-2018

Publisher's Note